Journal of Alloys and Compounds 882 (2021) 160570

Contents lists available at ScienceDirect

Journal of Alloys and Compounds

journal homepage: www.elsevier.com/locate/jalcom

Effects of solidification rate on the leaching behavior of metallic impurities in metallurgical grade silicon

Lu Zhou[a,b], Sheng Li[a], Qiwei Tang[b], Xiaocong Deng[a,b], Kuixian Wei[a,b,*], Wenhui Ma[a,b,c]

[a] National Engineering Laboratory for Vacuum Metallurgy, Kunming University of Science and Technology, Kunming 650093, PR China
[b] Faculty of Metallurgical and Energy Engineering, Kunming University of Science and Technology, Kunming 650093, PR China
[c] Engineering Research Center for Silicon Metallurgy and Silicon Materials of Yunnan Province, Kunming 650093, PR China

ARTICLE INFO

Article history:
Received 16 March 2021
Received in revised form 20 May 2021
Accepted 25 May 2021
Available online 2 June 2021

Keywords:
Metallurgical grade silicon
Solidification
Acid leaching
Refinement

ABSTRACT

Precipitation of the impurity phase during the solidification of metallurgical grade silicon melt determines the distribution law and occurrence state of impurities in silicon, while also determining the removal efficiency of impurities during the leaching process. In this research, distribution and occurrence states of inclusions in silicon at different solidification rates were detected via an electron probe microanalyzer (EPMA). Results have shown that the size of the inclusions becomes larger following electric resistance remelting, and some new impurity phases are generated, such as the VSi_2 phase, $TiSi_2$ phase, Si-Fe-Al-Ni-Zr phase, and $Si_{25}FeAl_2Ca_{16}NiCu_2$ phase. It is seen that there are clear boundaries between different phases. In addition, based on agitation leaching of 4.0 mol·L^{-1} HCl and 2.0 mol·L^{-1} HF mixed acid, it was found that most of the impurities in industrial silicon were effectively removed during this process. The impurities in the industrial silicon decreased from 5233.0 ppmw to 181.7 ppmw. The precipitation of the Si-Fe-Al-Ni-Zr (Cu) phase was the main factor providing improved efficiency of impurity removal, which exposed the impurity elements to the greatest extent. Industrial silicon was subjected to resistance remelting at different solidification rates, and the removal effects of impurities were also different. The impurity removal effect was optimal at a solidification rate of 1 °C/min, as the impurities were reduced to 131.9 ppmw.

1. Introduction

As a type of inexhaustible clean energy, solar energy is of great significance to energy resources and environments. Polysilicon is a main raw material for solar cell manufacturing, and its purity is required to reach at least 99.9999%. During the solidification of industrial silicon, impurity segregation is affected [1–7]. Lee et al. [8]. studied the behavior of metal impurities in silicon during each step of the smelting process. The different forms of inclusions led to different refinement behaviors. The high diffusion coefficient of copper allowed impurities to become easily extracted to the surface of silicon. The highest refining rate of copper was 97.95%, and the minimum refining rate of aluminum was 96.09%. Research by Brice et al. [9]. has indicated that a higher solidification rate will lead to insufficient time for the solute to precipitate and increasing the solidification rate will reduce the segregation of impurities in the melt.

Silicon demonstrates high corrosion resistance to any other acid, except HF acid. During the impurity leaching process, factors such as particle size of the silicon powder, pickling time, and acid concentration affect the impurity removal rate [10–14]. Sahu et al. [15]. studied the effects of changes in HCl solution on the removal of impurities in silicon, and the results showed that the impurity removal rate increased with increasing HCl concentration. Zeng et al. [16]. mixed HCl and HF for leaching and the removal rate of Fe impurities reached 99.7%, the removal rate of Ti reached 99.1%, the removal rate of Ca reached 98.2%, and the removal rates of Mg and Al were both 96.8%. Lai et al. [17]. performed wet purification of MG-Si using HF with H_2O_2 as the oxidant. It was found that when leaching with 1.0 mol·L^{-1} HF and 2.0 mol·L^{-1} H_2O_2, the purity of silicon increased from 99.74% to 99.96% in only 0.25 h, and then further increased to 99.99% over time.

The precipitation of the impurity phase during the solidification of silicon melt determines the distribution law and occurrence state of impurities in silicon, which will determine the removal efficiency of impurities during the process of wet leaching. During the process

* Corresponding author at: National Engineering Laboratory for Vacuum Metallurgy, Kunming University of Science and Technology, Kunming 650093, PR China.
E-mail address: kxwei2008@hotmail.com (K. Wei).

https://doi.org/10.1016/j.jallcom.2021.160570
0925-8388/

of synergistic removal of impurities by solidification refining and acid leaching of industrial silicon, most of the impurities with low solubility will be deposited in the cracks and at grain boundaries. When the solidified and refined industrial silicon is pulverized, the grain boundaries become exposed. Then, the remelted silicon was pickled and leached, and the impurities on the surface are effectively removed after pickling treatment [18–21]. Lu et al. [14]. studied the occurrence state and distribution law of inclusions in industrial silicon before and after refining and found that the leaching effects vary due to the differences in inclusion microstructure.

In this research, the best solidification rate was obtained by probing into the occurrence state and distribution law of impurities at the grain boundary under different solidification rates. Finally, following acid leaching, the impurity removal efficiency was investigated with the acid leaching experiment.

2. Experimental materials and methods

The raw material of this experiment was bulk industrial silicon, and its impurity content was tested and analyzed multiple times by inductively coupled plasma spectrometry (ICP-AES, PerkinElmer Avio500, America). The specific values are shown in Table 1. Fig. 1 for its measurement error. The experimental equipment was a vacuum tube resistance furnace, and the schematic diagram of the equipment is shown in Fig. 2. Two types of samples were prepared before the test. One was prepared as follows: industrial silicon was taken and placed in a crucible, heated up to 1500 °C for 1 h in a vacuum tube electric furnace with argon gas for complete melting, and cooled to 50 °C at decreasing temperature rates of 4 °C /min, 2 °C/min, 1 °C/min, and 0.5 °C/min, respectively. The sample was removed and pulverized, and the silicon wafer was polished with a metallographic polishing machine to observe the distribution and morphology of the precipitate. The microstructure and composition of secondary precipitates were tested using a scanning electron microscope (SEM, JSM-78, Japan) and an electron probe microanalyzer (EPMA-EDS, JXA8230, JEOL, Jpan). The second sample was prepared as follow: a crushed silicon briquette was pulverized to below 200 mesh with a ball mill, pickled, and immersed in a mixture of

Table 1
Concentration of main impurity elements in industrial silicon (ppmw).

Element	Fe	Al	Ca	Ti	V	Mn	Ni
Concentration (ppmw)	3200	1200	200	400	99	88	46

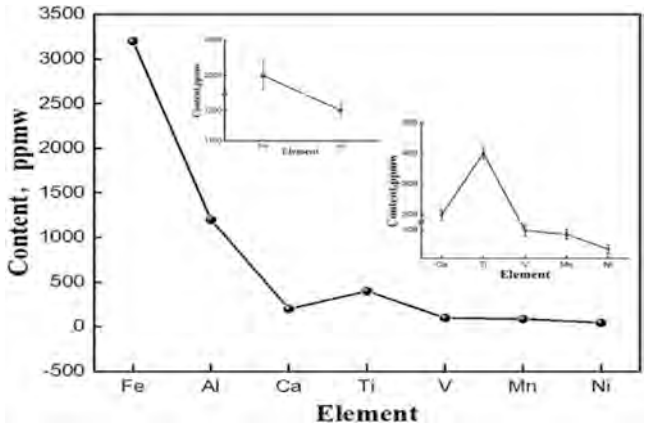

Fig. 1. Concentration of main impurity elements in industrial silicon (ppmw).

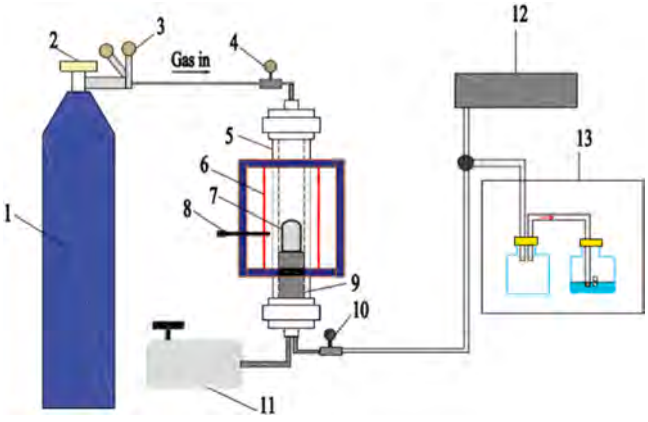

Fig. 2. 1 – Ar gas tank; 2 – Gas switch; 3 – Gas flow meters; 4 – Vacuum meter; 5 – Corundum tube; 6 – Silicon molybdenum rod heater; 7 – Samples; 8 – Thermocouple; 9 – Refractory brick; 10 – Vacuum meter; 11 – Vacuum pump; 12 – cooling device; 13 – inverted suction device.

4.0 mol·L^{-1} HCl and 2.0 mol·L^{-1} HF for four hours with magnetic stirring, filtered, rinsed with deionized water, and dried. It was carried out three times under the same operating conditions, and the impurity content in the silicon powder following acid leaching was detected with the ICP-AES.

3. Results and discussion

3.1. Microstructure of inclusions in industrial silicon

The secondary precipitated phases of inclusions in the industrial silicon were detected and analyzed by EPMA, and their composition is detailed in Table 2.

The microstructure of the inclusions in silicon is complex, and the color of the picture is obviously different due to the different compositions of the secondary precipitates in the inclusions. Dark gray, light gray, and light white impurity phases were randomly distributed in the inclusions.

First, the forms of inclusions in the industrial silicon are characterized, as shown in Fig. 3. According to the mapping results, elemental Fe and Al are almost enriched throughout the entire inclusion, but the enrichment degree of Fe is higher than that of Al on the whole, because the content of elemental Fe in the industrial silicon is higher than that of Al. Second, the presence of elemental V and Ti may be due to the similarity of the segregation coefficient and diffusion coefficient of Ti and V. In addition, the elemental Ca is only partially enriched in the impurity phase, and some Ti elements coexist with Si and Fe. The Mn and Ni elements are almost distributed in the entire impurity phase in the form of scattered dots, but the enrichment effect of Mn is significantly better than that of Ni, which is consistent with the ICP results of Mn and Ni in the industrial silicon. According to their atomic ratios, the impurity phases are estimated to be $FeSi_2$(Al), $FeSi_2Ti$, $Si_8Al_6Fe_4Ca$, and $Si_{30}Fe_4Al_5Ti_4V_5Ca$. The impurity phase $FeSi_2$ is light gray, and there is always a small amount of elemental Al in this phase. The impurity phase $FeSi_2Ti$ is shown as white lumps and randomly embedded throughout all inclusions. The impurity phase $Si_{30}Fe_4Al_5Ti_4V_5Ca$ exists in dark gray stripes. At the same time, according to the phase diagram and XRD database comparison, the phase is considered to be in the form of a mixture of $Si_8Al_6Fe_4Ca$, $TiSi_2$, and VSi_2.

Table 2
Chemical composition of typical inclusions in industrial silicon, at%.

Phase	Si	Fe	Al	Ca	Ti	V	Mn	Ni	Zr
$FeSi_2(Al)$	59.43	30.63	8.62				0.97	0.35	
$FeSi_2Ti$	48.61	23.92	1.76		22.29	2.07	0.82		0.53
$Si_8Al_6Fe_4Ca$	41.72	22.20	31.10	4.60			0.38		
$Si_{30}Fe_4Al_5Ti_4V_5Ca$	59.51	8.81	9.62	1.80	8.77	10.74	0.74		

3.2. Microstructure of inclusions in industrial silicon under different solidification rates

3.2.1. Microstructure of inclusions at a solidification rate of 0.5 °C/min

When the cooling rate was 0.5 °C/min, the composition of the secondary precipitated phase of inclusions in industrial silicon after solidification is detailed in Table 3.

After solidification and refining at a rate of 0.5 °C/min, the impurities are concentrated, as shown in Fig. 4(b). Mapping results show that the elemental Fe and Mn are almost fully distributed throughout the entire impurity phase, where the elemental Fe is highly enriched, and Mn and Ni are distributed in the form of scattered points. Al and Ni are no longer concentrated in the inclusions because the impurities have enough time to diffuse and react to form different impurity phases after the cooling rate has been reduced. The Ti and V elements coexist, and the content of Ti element is significantly increased and relatively concentrated. This may be due to the replacement of a portion of V by Ti. Elemental Ca only occurs in $Si_8Al_6Fe_4Ca$. Compared with the industrial silicon, it is found that the contents of all elements in this phase are similar, and there is almost no change, indicating that the $Si_8Al_6Fe_4Ca$ phase is relatively stable. Based on EPMA detection and analysis, it was found that the content of Al in the impurity phase $FeSi_2$ significantly decreased from 8.62% to 5.91% in the industrial silicon. In addition, the color intensity of the impurity phase $FeSi_2Ti$ is more obvious, which is attributed to the relative increase in Ti content. The $Si_8Al_6Fe_4Ca$, $TiSi_2$, VSi_2 impurity phases appear separately, and no longer occur in the form of a mixture.

Table 3
Chemical composition of typical inclusions in silicon with a solidification rate of 0.5 °C/min, at%.

Phase	Si	Fe	Al	Ca	Ti	V	Mn	Ni
$FeSi_2(Al)$	62.42	30.82	5.91				0.85	
$FeSi_2Ti$	48.61	24.97	0.86		24.81		0.76	
$Si_8Al_6Fe_4Ca$	40.29	22.89	30.73	5.07			0.49	0.53
$TiSi_2$;VSi_2	65.30	2.02	0.80		11.74	19.44	0.70	

3.2.2. Microstructure of inclusions at a solidification rate of 1 °C /min

When the cooling rate was 1 °C/min, the composition of the secondary precipitated phase of inclusions is detailed in Table 4.

After solidification and refining at a rate of 1 °C/min, new impurity phases, Si-Fe-Al-Ni-Zr, $Si_{25}FeAl_2Ca_{16}NiCu_2$, Si_9FeTi_3V, appeared on the basis of common impurity phases, as shown in Fig. 5(b). According to the mapping results, Fe, Al, Mn, and Ni are mostly distributed throughout the impurity phase. However, no Mn

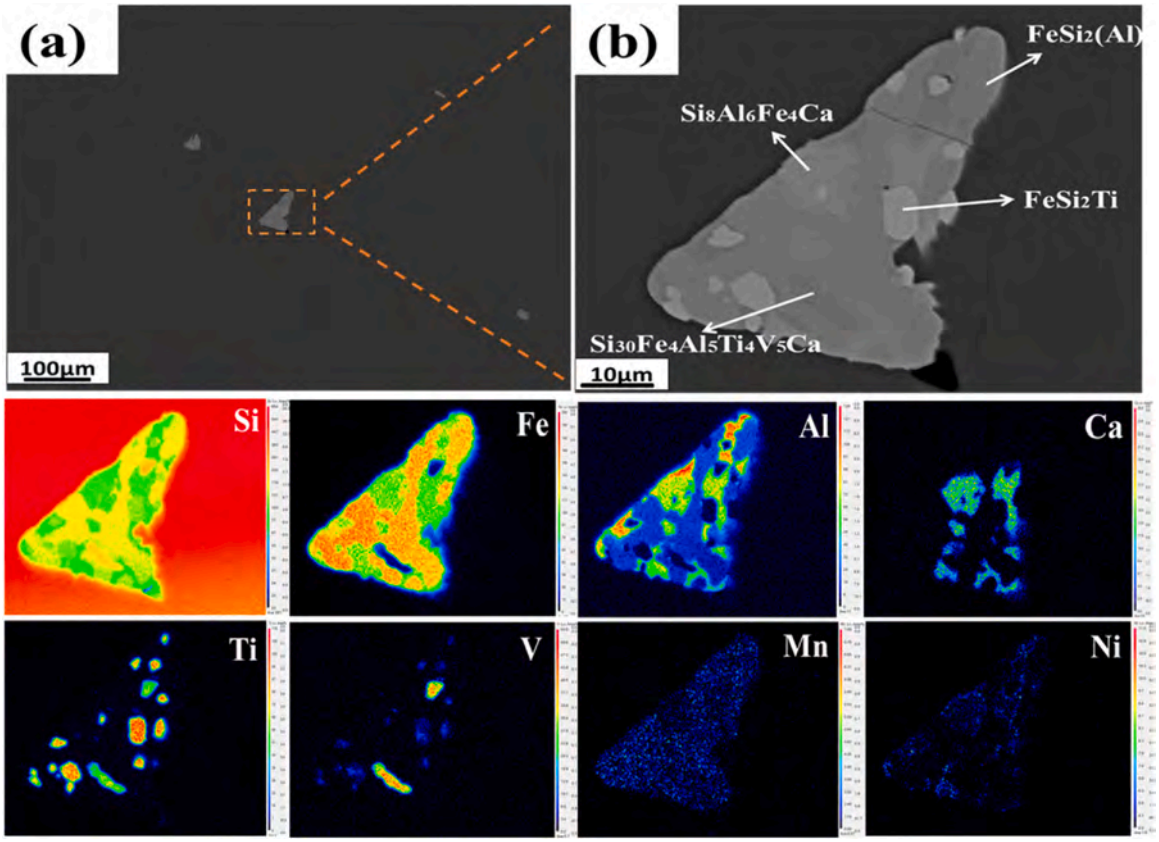

Fig. 3. Microstructure of industrial silicon and EPMA analysis of representative impurities.

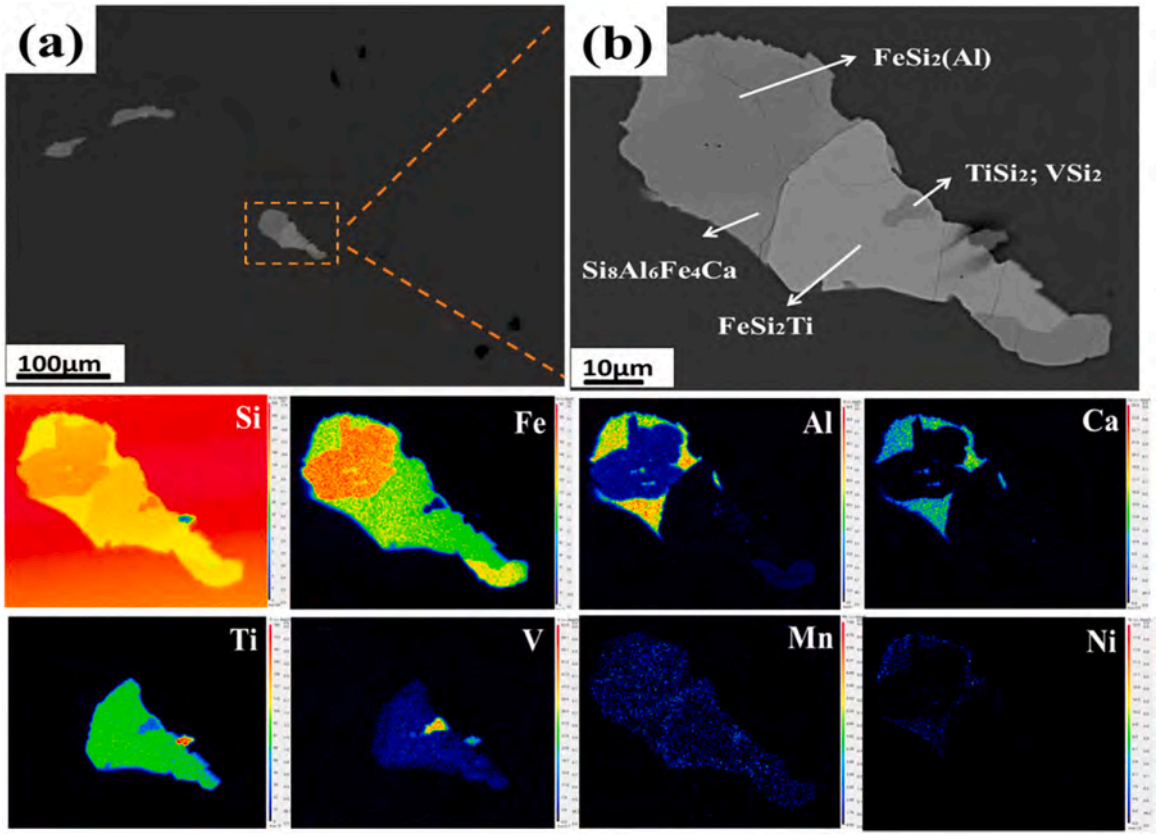

Fig. 4. The microstructure of silicon with a solidification rate of 0.5 °C/min and EPMA analysis of representative impurities.

Table 4
Chemical composition of typical inclusions in silicon with a solidification rate of 1 °C /min, at%.

Phase	Si	Fe	Al	Ca	Ti	V	Mn	Ni	Zr	Cu
$FeSi_2$(Al)	62.37	31.07	5.40	0.21			0.96			
$Si_8Al_6Fe_4Ca$	41.79	21.83	29.16	5.73			0.84	0.65		
Si-Fe-Al-Ni-Zr;$TiSi_2$	52.50	25.22	12.75	1.42	2.90			2.33	2.88	
$Si_{25}FeAl_2Ca_{16}NiCu_2$	50.01	2.84	5.68	32.66				2.16		6.65
$TiSi_2$;VSi_2;FeSi	62.90	7.49	0.38		21.85	6.95	0.42			

element can be found in any phase containing Cu or Zr. In addition, the enrichment of Ni is higher than that of Mn. This is because a portion of Ni occurs in the impurity in a dispersed form, and a portion forms the $Si_{25}FeAl_2Ca_{16}NiCu_2$ and Si-Fe-Al-Ni-Zr phases. The Ti and V are still present and relatively concentrated in most cases, but in the Si-Fe-Al-Ni-Zr phase, there is some Ti enrichment without V. It was found that a higher Cu content was found in the composition of $Si_{25}FeAl_2Ca_{16}NiCu_2$ through EPMA inspection, which may be due to the smaller segregation coefficient of Cu in Si. As the Al content in the $FeSi_2$ phase was further reduced, the color presented was darker. In the Si-Fe-Al-Ni-Zr and $TiSi_2$ phases, the presence of elemental Zr causes the phase to appear bright gray in the backscattered state. $Si_8Al_6Fe_4Ca$ is the main precipitation phase, while $Si_{25}FeAl_2Ca_{16}NiCu_2$ and Si-Fe-Al-Ni-Zr are embedded in the larger precipitation phase $Si_8Al_6Fe_4Ca$ in the inclusions. According to its atomic ratio, it is speculated that Si_9FeTi_3V occurs in the form of a mixture of $TiSi_2$, VSi_2, and FeSi. The content of Al in this impurity phase is lower, and the concentration of Ti increases. According to atomic orbital theory, the outermost electron of the Al element is the 3P orbital, while that of Ti is the 3d orbital. Therefore, the activity of Ti atoms is relatively high, and the affinity of Si for Ti is greater than the affinity of elemental Si for Al.

3.2.3. Microstructure of inclusions at a solidification rate of 2 °C/min

When the cooling rate was 2 °C/min, the composition of the secondary precipitated phase of inclusions is detailed in Table 5.

When the solidification rate was 2 °C/min, the precipitate is more uniformly distributed in the remelted industrial silicon, as shown in Fig. 6(b). The impurity phases primarily include the $FeSi_2$, $FeSi_2Ti$, $Si_8Al_6Fe_4Ca$, and $Si_7Al_8Fe_5$ phases. However, the size of the inclusions is significantly larger than the size of the industrial silicon inclusions, and the shape is transformed from a smaller block to a long block. Moreover, the boundary between phases is clearer. According to the mapping diagram, it can be found that the elemental Ca only occurs in the $Si_8Al_6Fe_4Ca$ phase and is relatively concentrated. The elemental V always appears in the Ti-rich region, which is due to the lower segregation coefficient and higher diffusivity of the Ti and V. However, after analyzing the results of EPMA, it was found that the elemental V in the $FeSi_2Ti$(V) phase may be caused by the substitution for some Ti elements. The Al element in the $FeSi_2$(Al) phase in the inclusions increased to 8.76%, further indicating that the Al element does occur in the form of dissolved Al. As a common impurity phase in silicon, the $Si_8Al_6Fe_4Ca$ phase is very stable during the solidification process, and its proportion hardly changes. However, as the solidification rate increases, this phase is significantly

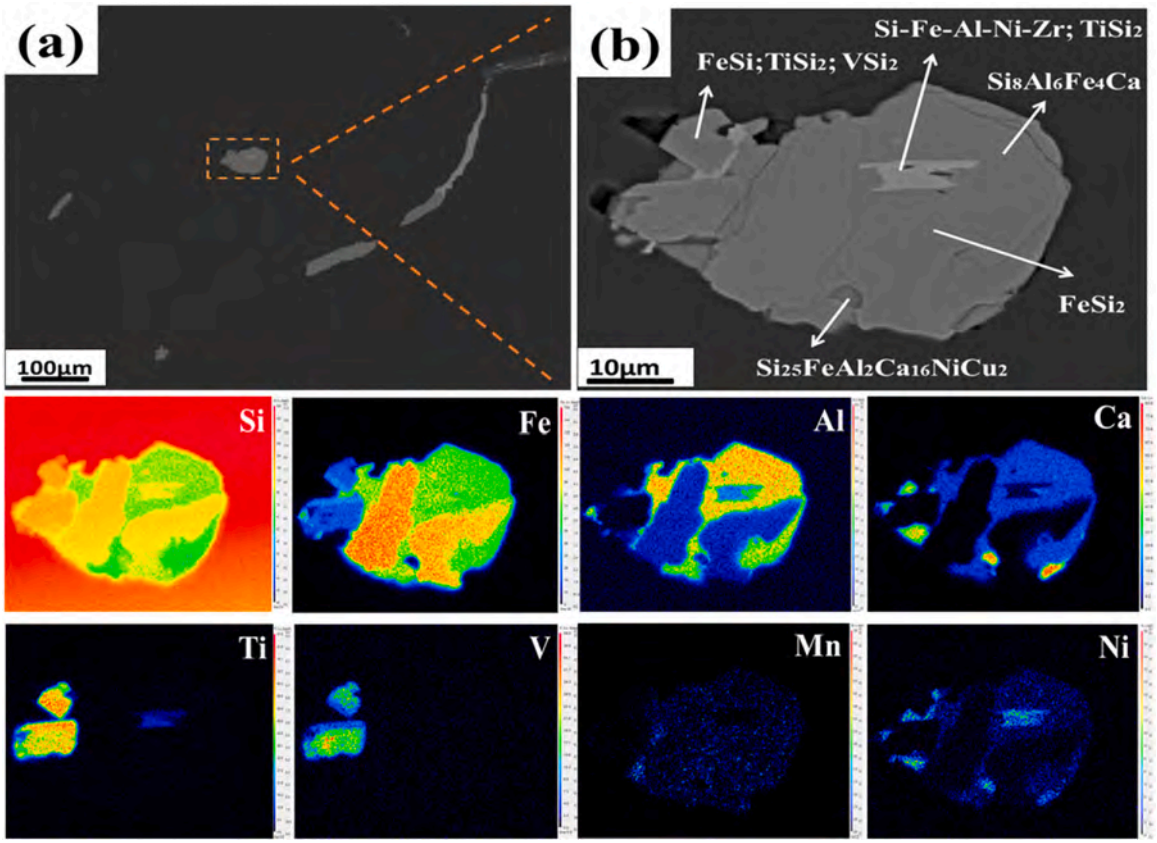

Fig. 5. The microstructure of silicon with a solidification rate of 1 °C/min and EPMA analysis of representative impurities.

more concentrated in the inclusions. The $Si_7Al_8Fe_5$ phase occurred as a new phase, possibly due to the fact that the $FeSi_2$ (Al) phase gradually evolved into $Si_7Al_8Fe_5$ as the solidification process proceeded.

3.2.4. Microstructure of inclusions at a solidification rate of 4 °C/min

When the cooling rate was 4 °C/min, the composition of the secondary precipitated phase of inclusions is detailed in Table 6.

Industrial silicon was remelted at a cooling rate of 4 °C/min. The mapping in Fig. 7 shows that Fe, as the impurity of the highest concentration in industrial silicon, is almost concentrated throughout the entire impurity phase, while elemental Al was relatively concentrated, mostly in the $Si_7Al_8Fe_5$ phase. No dissolved Al occurred in the independent phase of $FeSi_2$. The white lumpy $FeSi_2Ti$ phase precipitates in two places, but the composition is quite different between the two. The thick and lumpy $FeSi_2Ti$ phase showed no element Al but it contained a small amount of elemental Zr, thus appearing as bright white. No elemental Ca enrichment was found in the inclusions, which is probably due to the evaporation of elemental Ca. The precipitated phases $FeSi_2Ti$, $TiSi_2$, and VSi_2 enriched in Ti and V changed from the original block shape to the strip shape as a result of the accelerated solidification rate. The elemental Mn was scattered throughout the inclusions in the form of scattered points. At the same time, based on an analysis of the EPMA results, elemental V only appears in VSi_2, and there is no elemental V in the $FeSi_2Ti$ phase, indicating that the V does not replace Ti at this solidification rate.

According to the above experiment, it can be seen that when industrial silicon is cured and purified at different rates, and its size is significantly larger than that of the industrial silicon inclusions, and the boundary between the phases is clearer. As is shown in Fig. 8. Fe and Mn were found to be almost fully distributed throughout the impurity phase. Fe was highly enriched, Mn and Ni were distributed in the form of scattered points, while Ti and V coexisted. After solidification and refining, some new impurity phases appeared, such as the $TiSi_2$, VSi_2, and $Si_7Al_8Fe_5$ phases. In particular, when the solidification rate was 1 °C/min, the inclusion phase containing Cu and Zr appeared. Under these conditions, the impurity phase precipitated as much as possible and was more conducive to the subsequent acid leaching process for impurity removal.

3.3. Morphological mechanism of inclusions in silicon

In metallurgy, there are many parameters that affect the removal of metal impurities, such as solidification rate, impurity segregation coefficient, diffusion coefficient, etc., but the optimal range of these parameters and the degree of impact on the removal of impurities are still unclear. This chapter calculates and analyzes the influence of

Table 5
Chemical composition of typical inclusions in silicon with a solidification rate of 2 °C/min, at%.

Phase	Si	Fe	Al	Ca	Ti	Mn	Ni	Zr	Cu
$FeSi_2$(Al)	58.98	31.25	8.76			1.00			
$FeSi_2Ti$	47.64	25.09	1.68		24.08	0.93		0.60	
$Si_8Al_6Fe_4Ca$	40.78	22.28	30.87	5.06		0.44	0.56		
$Si_7Al_8Fe_5$	35.14	24.44	38.45		0.17	0.90	0.67		0.23

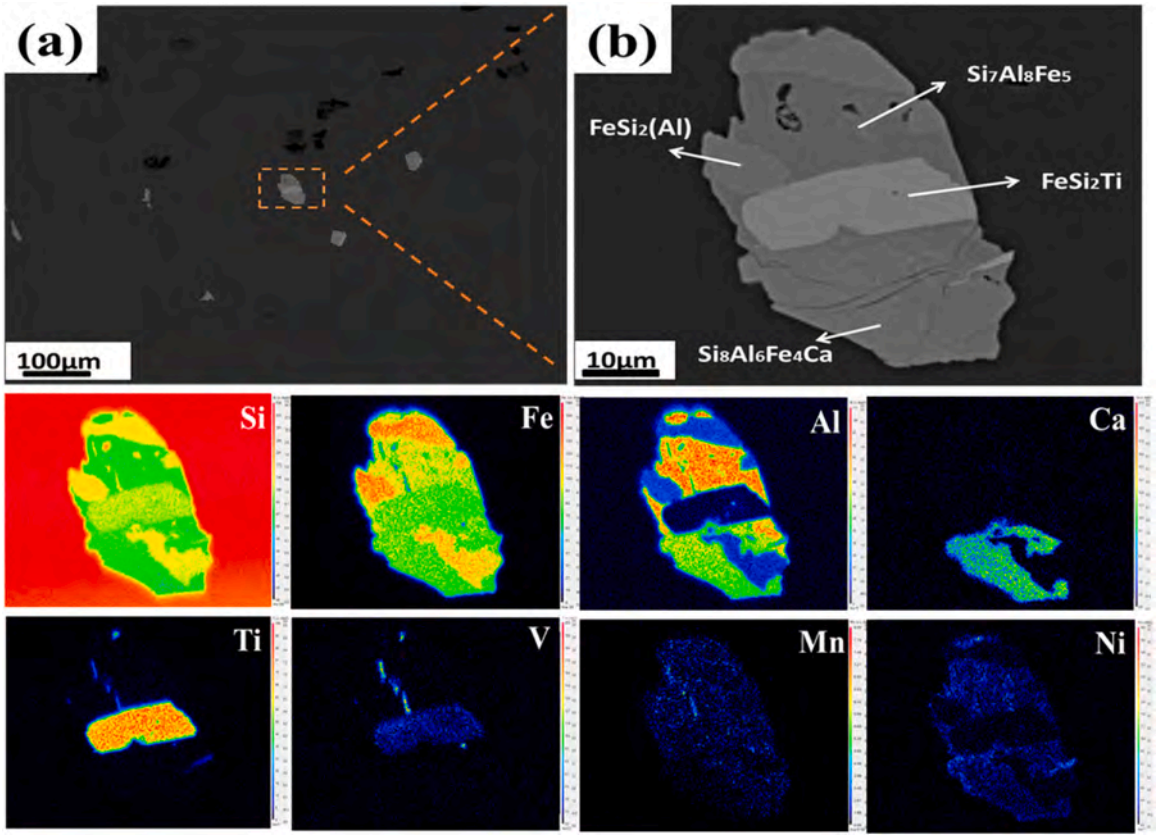

Fig. 6. Microstructure of silicon with a solidification rate of 2 °C/min and EPMA analysis of representative impurities.

Table 6
Chemical composition of typical inclusions in silicon with a solidification rate of 4 °C/min, at%.

Phase	Si	Fe	Al	Ti	V	Mn	Ni	Zr
$FeSi_2$	67.55	31.65				0.79		
$FeSi_2Ti$	48.32	24.21		23.84		1.91		1.72
$Si_7Al_8Fe_5$	35.28	23.25	39.58			0.90	1.00	
$FeSi_2Ti$	54.07	21.27	2.45	21.10		0.56		
$FeSi_2$;$TiSi_2$;VSi_2	56.73	12.42	6.54	20.11	3.63	0.56		

temperature on the distribution of metallic impurities in silicon starting from the binary phase diagram and diffusion coefficient of metallic impurities in silicon. As is shown in Fig. 9. Metal impurities rarely exist in an interstitial or substitutional state in silicon crystals, and most of them may precipitate together with other impurities in the form of precipitates or metal silicides. From the perspective of the phase diagram, Fe forms the silicide $FeSi_2$, Ti forms the silicide $TiSi_2$, and Ca forms the silicide $CaSi_2$. However, in the actual experimental process, due to the joint action of other factors, there are some differences between the theoretical results and the existence form of the precipitate.

The diffusion rates of metal impurities are different, and the types of formed inclusions will be different with varying solidification rates. According to the Stokes formula, the diffusion coefficient of impurities in the silicon melt is considered to be related to the atomic radius of the impurity, which can be calculated by the following formula:

$$D = \frac{k_B T}{6\pi\eta\gamma_0} \quad (1)$$

where D is the diffusion coefficient of the impurity atom, η is the viscosity, and γ_0 is the atomic radius.

Silicon melt viscosity can be expressed as: $\lg \eta = \frac{819}{T} - 0.727$. The melting point viscosity is 0.57 mPa•s.

Fig. 10 is obtained by the corresponding calculation:

Table 7 shows the diffusion coefficient of the main metal impurities in the silicon system at the melting point of silicon.

It can be seen from the above analysis that diffusion is related to the temperature of the experiment. Increasing the temperature within a certain range can increase the diffusion coefficient of impurities, which in turn facilitates the precipitation of impurities and improves the removal rate of impurities.

3.4. The leaching effect of metallurgical grade silicon under different solidification rates

As shown in Fig. 11, the five groups of samples prepared at different solidification rates were ground to below 200 mesh, stirred for 6 h in a mixed solution of 4.0 mol·L^{-1} HCl and 2.0 mol·L^{-1} HF at 60 °C, filtered with suction, and washed with deionized water. The concentration of impurities of the industrial silicon after acid leaching was reduced to 181.7 ppmw, and the impurity concentrations after solidification at cooling rates of 0.5 °C/min, 1 °C/min, 2 °C/min, and 4 °C/min combined with acid leaching treatment were 162.6 ppmw, 131.9 ppmw, 204.5 ppmw, and 222.1 ppmw, respectively. The impurity removal efficiencies of acid leaching samples with cooling rates of 2 °C/min and 4 °C/min were lower than that of industrial silicon after acid leaching. The reason may be that the precipitation of main metal impurities decreases with increasing solidification rate. In other words, the main metal impurities have solidified before they sufficiently diffuse. It should be pointed out that a solidification rate of 0.5 °C/min is not optimal and attributable to the formation of back-diffusion as a result of the too slow solidification rate. Based on the mapping under corresponding conditions, it was found that after the resistance remelting of Ca with a

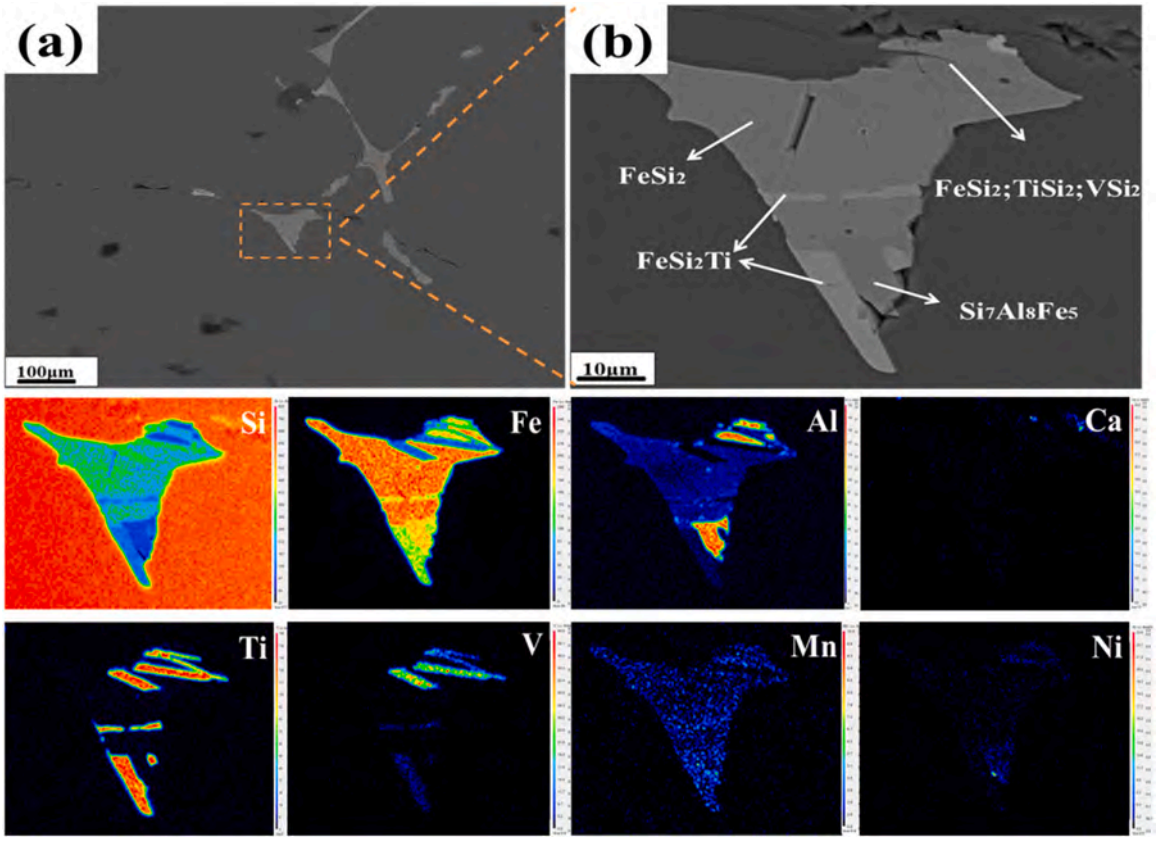

Fig. 7. The microstructure of silicon with a solidification rate of 4 °C/min and EPMA analysis of representative impurities.

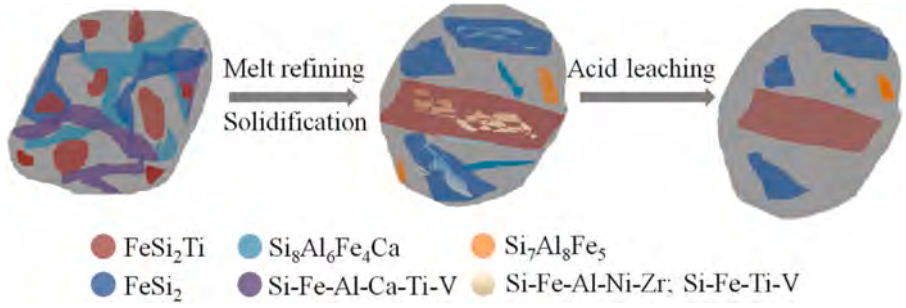

Fig. 8. Schematic diagram of impurity removal by solidification and acid leaching : different colors represent different phases.

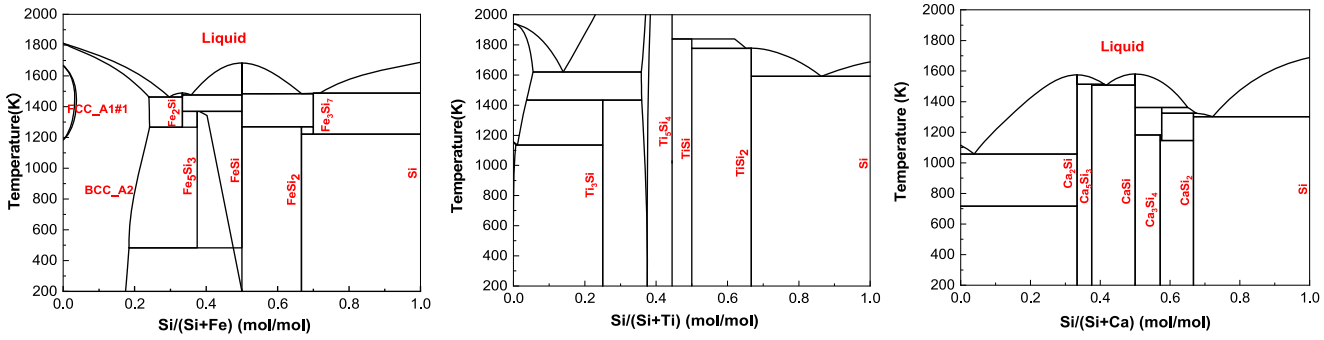

Fig. 9. Binary phase diagram of some common impurities in silicon. (a) Si-Fe binary alloy phase diagram; (b) Si-Ti binary alloy phase diagram; (c) Si-Ca binary alloy phase diagram.

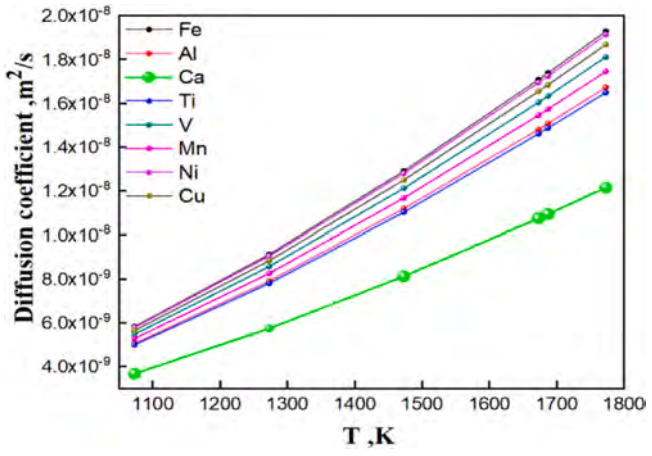

Fig. 10. Diffusion coefficient of the impurity in silicon.

Table 7
The diffusion coefficient of the main metal impurities in the silicon system at the melting point of silicon.

Element	Atomic radius (m)	D ($cm^2 \cdot s^{-1}$)
Fe	1.24×10^{-10}	1.738×10^{-8}
Al	1.43×10^{-10}	1.507×10^{-8}
Ca	1.97×10^{-10}	1.094×10^{-8}
Ti	1.45×10^{-10}	1.486×10^{-8}
V	1.32×10^{-10}	1.632×10^{-8}
Mn	1.37×10^{-10}	1.573×10^{-8}
Ni	1.25×10^{-10}	1.724×10^{-8}
Cu	1.28×10^{-10}	1.683×10^{-8}

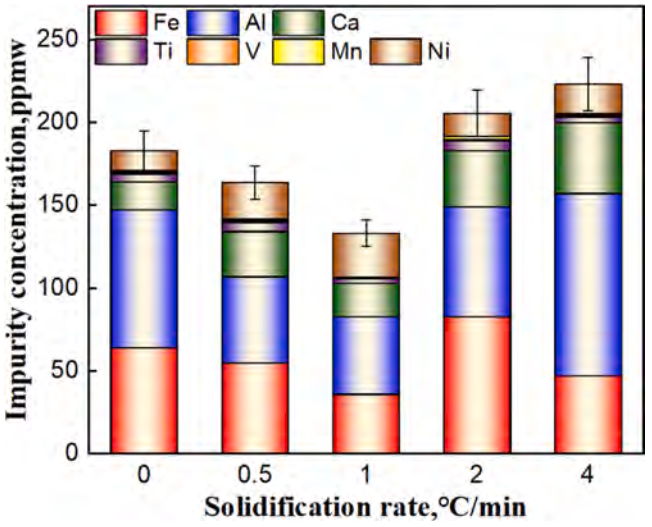

Fig. 11. Impurity content of different samples combined with acid leaching.

solidification rate of 4 °C/min, no Ca segregation enrichment was found, which may have been caused by the evaporation of Ca. After acid leaching, the content of Ti decreased to a few ppmw because Ti is often segregated in silicon as $FeSi_2Ti$ or $TiSi_2$. In addition, after acid leaching, the concentration of V (< 5.0 ppmw) was as low as the detection limit. The removal efficiency for Mn impurities was also rather high, where all concentrations were reduced to approximately 1.0 ppmw. The removal effect for Ni is poor, which is consistent with the results of EPMA, and Ni has no significant precipitation and enrichment under different solidification rates.

4. Conclusions

The inclusions in industrial silicon are randomly distributed in small blocks. After resistance remelting at different solidification rates, the sizes of the inclusions become larger, the enrichment of the same type of impurity phase is more concentrated, and the boundary is distinct. At the same time, inclusion phases containing Ti, V, Ni, Cu, and Zr were precipitated, which is beneficial to the subsequent wet removal of impurities. After stirring and leaching with the mixed acid solution of 4.0 $mol \cdot L^{-1}$ HCl and 2.0 $mol \cdot L^{-1}$ HF, the impurities in the industrial silicon decreased from 5233.0 ppmw to 181.7 ppmw. After remelting and solidification at different solidification rates, all impurities were properly removed. The impurity removal result was the best at a solidification rate of 1 °C/min, as the impurities were reduced to 131.9 ppmw. The precipitation of the Si-Fe-Al-Ni-Zr (Cu) phase was the main factor to improving the impurity removal efficiency, which exposed the impurity elements to the greatest extent.

CRediT authorship contribution statement

Lu Zhou: Experimental, Data curation, Writing - original draft, Validation. **Sheng Li:** Methodology. **Qiwei Tang:** Visualization. **Xiaocong Deng:** Software. **Kuixian Wei:** Supervision. **Wenhui Ma:** Conceptualization.

Declaration of Competing Interest

The authors declare that they have no known competing financial interests or personal relationships that could have appeared to influence the work reported in this paper.

Acknowledgments

This research was financially supported by the Joint Foundation (No. U1902219) and the Reserve Talents of Young and Middle-aged Academic and Technical Leaders in Yunnan Province (No. 2018HB009).

References

[1] X.L. Bai, B.Y. Ban, J.W. Li, Z.Q. Fu, Z.J. Peng, C.B. Wang, J. Chen, Segregation behavior of metal impurities during Al-Si melt directional solidification with an open ended crucible, Silicon 10 (2018) 1283–1290.
[2] F. Huang, R.R. Chen, J.J. Guo, H.S. Ding, Y.Q. Su, Removal of metal impurities in metallurgical grade silicon by cold crucible continuous melting and directional solidification, Sep. Purif. Technol. 188 (2017) 67–72.
[3] W.Z. Yu, Y. Xue, J. Mei, X.Z. Zhou, M.L. Xiong, Segregation and removal of transition metal impurities during the directional solidification refining of silicon with Al-Si solvent, J. Alloy. Compd. 805 (2019) 198–204.
[4] Q.C. Zou, N. Han, Z.X. Zhang, J.C. Jie, F. Xu, X.Z. An, Metals 10 (2020) 155.
[5] N.S. Ganesan, S. Manickam, A. Karuppanan, R. Perumalsamy, Simulation analysis on impurity distribution in mc-Si grown by directional solidification for solar cell applications, Int. J. Mater. Res. 107 (2016) 525–533.
[6] W.Y. Wang, S. Shi, P.T. Li, D.C. Jiang, Y. Yang, J.Y. Li, Y. Tan, H.M. Noor ul Huda Khan Asghar, Exploration on the removal of arsenic in silicon under electron beam melting condition, Vacuum 166 (2019) 191–195.
[7] J.F. Hu, K.S. Zhu, K.X. Wei, W.H. Ma, T.L. Lv, Effects of pulling rate on metal impurity removal during Si refining in Ti-90 wt% Si alloy directional solidification, J. Alloy. Compd. 816 (2020) 152621.
[8] W. Lee, J. Kim, B. Jang, Y. Ahn, H. Lee, W. Yoon, Refining of MG-Si by hybrid melting using steam plasma and EMC, Sol. Energy Mater. Sol. Cells 95 (2011) 56–58.
[9] J.C. Brice, The variation of interface segregation coefficients with growth rate of crystals, J. Cryst. Growth 10 (1971) 205–206.
[10] K.X. Wei, S.C. Yang, X.H. Wan, W.H. Ma, J.J. Wu, Y. Lei, Review of silicon recovery and purification from saw silicon powder, JOM 72 (2020) 2633–2647.
[11] H.X. Lai, L.Q. Huang, C.H. Gan, P.F. Xing, J.T. Li, X.T. Luo, Enhanced acid leaching of metallurgical grade silicon in hydrofluoric acid containing hydrogen peroxide as oxidizing agent, Hydrometallurgy 164 (2016) 103–110.
[12] F. Ebrahimfar, M. Ahmadian, Purification of metallurgical-grade silicon by acid leaching, Silicon 11 (2019) 1979–1987.

[13] S. Espelien, G. Tranell, J. Safari Energ. Technol. (2017) 355–365.
[14] H.F. Lu, K.X. Wei, W.H. Ma, K.Q. Xie, J.J. Wu, Y. Lei, The effect of secondary refining on the removal of phosphorus from metallurgical-grade silicon by acid leaching, Met. Mater. Trans. B 48 (2017) 2768–2780.
[15] S.K. Sahu, E. Asselin, Effect of oxidizing agents on the hydrometallurgical purification of metallurgical grade silicon, Hydrometallurgy 121–124 (2012) 120–125.
[16] R. Zeng, Y.H. Wang, J.X. Zhang, J.Q. Xu, H.Y. Li, X.F. Chen, W.D. Xing, Hydrometallurgical purification of metallurgy grade silicon by acid leaching, Adv. Mater. Res. 549 (2012) 428–431.
[17] H.X. Lai, L.Q. Huang, H.P. Xiong, C.H. Gan, P.F. Xing, J.T. Li, X.T. Luo, Ind. Eng. Chem. Res. 56 (2017) 311–318.
[18] X.H. Cui, S.N. Jiang, K.C. Dong, X. Jin, J. Zhao, P.F. Xing, X.H. Du, Refractories 6 (2018) 459–462.
[19] T.Y. Li, L. Guo, Z. Wang, Z.C. Guo, Purification of metallurgical-grade silicon combining Sn–Si solvent refining with gas pressure filtration, RSC Adv. 10 (2020) 11435–11443.
[20] X. Jin, J. Kong, X.T. Zhou, P.F. Xing, Y.X. Zhuang, Recycling of silicon kerf loss derived from diamond-wire saw cutting process to prepare silicon nitride, J. Clean. Prod. 247 (2020) 119163.
[21] L.K. Liu, P.J. Niu, B.H. Huang, L. Chai, J.M. Zheng, X.L. Deng, L. Song, W.Q. Chen, Z.H. Yue, L. Zhou, H. Tang, Silicon-based anode materials with three-dimensional conductive network for high-performance lithium ion batteries, Inter. J. Nanomanuf. 15 (2019) 118–126.